Energy Proceedings
Vol 51, 2025
ISSN 2004-2965

Cost-Effective Hydrogen Storage Materials: Utilizing Biogas Slurry to Synthesize High-Performance Hollow porous Carbon Spheres#

Hang Yuan[1,2], Hongguang Zhu[1,2*], Longlong Lei[1,2], Man Sun[1,2]
1 School of Mechanical Engineering, Tongji University, Shanghai 201804, China
2 Bio-Energy Research Center, Institute of New Rural Development, Tongji University, Shanghai, 201804, China
Corresponding Author: zhuhg@tongji.edu.cn

ABSTRACT

Achieving a balance between cost-effectiveness and high performance in hydrogen storage materials is a significant challenge. This study presents a novel method for synthesizing hollow porous carbon spheres with a cluster-like structure using economical materials such as biogas slurry, starch, and ferric oxide. Through a systematic analysis of activation temperatures and ratios, optimal conditions were identified. The resulting materials, CS850-4.5 and CS800-4, achieved high gravimetric H_2 uptake of 4.5 wt% (77 K, 50 bar) and volumetric H_2 uptake of 25.9 g/L (77 K, 30 bar), respectively. This approach offers dual advantages in both performance and economic viability.

Keywords: Hydrogen Storage, Biogas Slurry, Hollow Porous Carbon Spheres, Cost-Effectiveness

NONMENCLATURE

Abbreviations	
CSm-n	Carbon Spheres m-n
Symbols	
ρ_g/ ρ_s/ ρ_p	Gas/ Skeletal/ Packing density (g cm^{-3})
m	Temperature (°C)
n	KOH-to-CS mass ratio

1. INTRODUCTION

Hydrogen is widely regarded as a viable energy carrier of the future due to its high energy density (142 MJ/kg), abundance, non-toxicity, and environmental friendliness.[1] However, traditional hydrogen storage methods, such as high-pressure gaseous storage and cryogenic liquid storage, face challenges in achieving compact, economical, and safe storage.[2] Solid-state hydrogen storage technology is considered a promising alternative, especially carbon-based porous materials derived from waste organic matter, which offer the potential for more efficient and economical hydrogen storage solutions. [3]

Biogas slurry, a complex and cost-effective byproduct produced during anaerobic fermentation, poses substantial challenges due to its large volume and disposal difficulties. Although current treatment methods for biogas slurry include land application as fertilizer and microalgae cultivation, these approaches do not fully address all the associated issues. The presence of heavy metals and antibiotics in the slurry can still pose potential food safety and environmental risks.[4]

Exploring the use of biogas slurry in the preparation of carbon-based hydrogen storage materials is a novel approach. As a high-carbon-content liquid organic matter, biogas slurry easily forms carbon-coated structures, making it an excellent carbon source for preparing hollow carbon materials, such as hollow porous carbon spheres.[5] These materials possess unique hollow structures and surface activity, providing a large specific surface area and excellent hydrogen encapsulation capabilities. Additionally, the abundant heteroatoms and other elements in biogas slurry may provide more active sites for adsorption. These features offer valuable insights for the development of low-cost, high-performance hydrogen storage materials. [6]

2. MATERIAL AND METHODS

2.1. Sample preparation

Add 6 g soluble starch and 4 g α-Fe_2O_3 to a mixture of 80 mL biogas slurry and 20 mL deionized water. Stir the mixture at 40°C for 2 h. Transfer the mixture into a PTFE-lined stainless steel autoclave and perform hydrothermal carbonization at 200°C for 7 hours. After cooling, dry the mixture to obtain a brownish-red powder, named CFe-HTC.

This is a paper for the 16th International Conference on Applied Energy (ICAE2024), Sep. 1-5, 2024, Niigata, Japan.

Place CFe-HTC in an alumina crucible and heat to 800°C under a N_2 atmosphere for 2 h to form a carbon-coated iron structure. After cooling, wash with deionized water, 1 mol/L HCl, and ethanol until the filtrate is clear, forming hollow carbon spheres. The dried black powder is named CS.

For KOH impregnation activation, mix KOH with 2g of CS at different ratio and ultrasonicate at 95°C for 30 minutes. Transfer the mixture to an alumina crucible, heat to various temperatures (800°C to 900°C) under N_2, and hold for 2 hours. After cooling, wash and dry the samples, then grind into a fine black powder, named CSm-n, where n is the KOH-to-CS mass ratio, and m is the activation temperature.

2.2. Characterization

The samples were characterized using Scanning Electron Microscopy (SEM), Transmission Electron Microscopy (TEM), Raman Spectroscopy, X-ray Diffraction (XRD), X-ray Photoelectron Spectroscopy (XPS), Fourier Transform Infrared Spectroscopy (FTIR), and N_2 adsorption-desorption isotherms (ASAP 2460 sorption analyzer). The surface area was calculated using the Brunauer-Emmett-Teller (BET) theory. The pore size distribution was analyzed by Density Functional Theory (DFT) and the Horvath-Kawazoe (HK) methods.

2.3. Hydrogen Adsorption Measurement

Hydrogen adsorption experiments were conducted using a BSD-VVS&DVS gravimetric vapor adsorption analyzer. Samples were degassed at 200°C for 3 hours, followed by measuring the hydrogen adsorption isotherms at 77K over a pressure range of 0-50 bar. The equilibrium time for each pressure point was 1 hour. The excess adsorption isotherms were primarily fitted using the ternary Langmuir model:

$$V_{excess} = \frac{V_L P}{P_L + P} \times \left(1 - \frac{\rho_g}{\rho_a}\right)$$

The skeletal density was measured using a BSD-TD true density analyzer.

3. RESULT AND DISCUSSION

3.1. Influence of Activation Temperature and KOH Ratio on the Textural Properties

Table 1 Textural properties of CSm-n at different activation temperatures (m) and activation ratios (n).

Sample	S_{BET} (m^2/g)	S_{micro} (m^2/g)	V_{total} (m^3/g)	V_{micro} (m^3/g)	D_{ave} (nm)
CS800-2	960	323	0.78	0.2	3.27
CS800-3	1244	379	1.06	0.18	3.43
CS800-4	1314	331	0.85	0.14	2.57
CS800-4.5	1688	622	1.78	0.56	4.22
CS800-5	1650	341	1.55	0.39	3.75
CS850-4.5	2142	1522	1.39	1.00	3.38
CS900-4.5	1981	716	1.45	0.38	2.93

As shown in Table 1, at 800°C, BET surface area of the material increases with the activation ratio n, reaching a maximum of 1688 m2/g at n=4.5. Furthermore, the micropore surface area, total pore volume and micropore volume of CS800-4.5 are also higher than those at lower n values. However, when n=5, the material's performance begins to decline, possibly due to excessive activation leading to the transition of micropores to mesopores and the collapse of the pore structure.

Maintaining an activation ratio of n=4.5, changing the activation temperature from 800°C to 900°C reveals that at 850°C, CS850-4.5 exhibits the highest BET surface area, with a micropore surface area reaching 1522 m^2/g. Although the total pore volume is lower than that of CS800-4.5 and CS900-4.5, its micropore volume reaches 1 m^3/g, indicating that the pores are predominantly microporous. Thus, an activation temperature of 850°C and a ratio of n=4.5 are identified as the optimal activation conditions for achieving higher hydrogen storage potential.

3.2. Morphological and structural characterizations

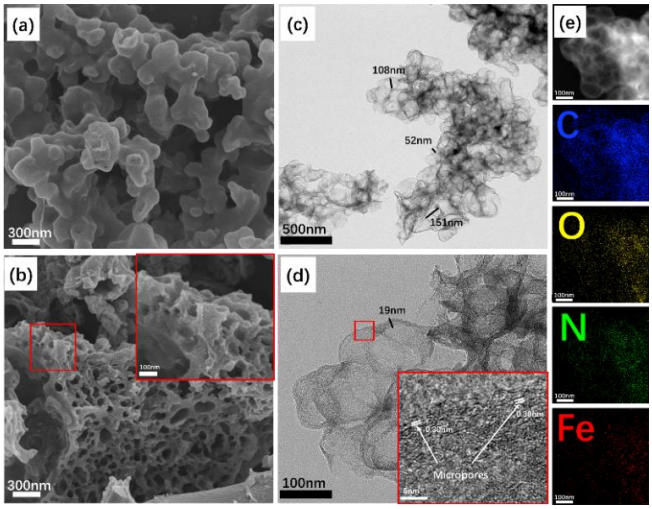

Fig. 1. (a, b) SEM images of CS850-4.5; (c, d, e) TEM images of CS850-4.5.

As observed in Fig. 1(a) and (b), the sample primarily exhibits a cluster-like sphere morphology. These spheres are not standard but irregular ellipsoids interconnected with each other. The numerous voids at the cross-section further confirm the cluster structure of hollow spheres.

According to Fig. 1(c) and (d), the diameter of individual hollow spheres ranges from approximately 50 to 150 nm, with a shell thickness of 15-20 nm. There are numerous micropores of 0.3-0.4 nm on the shell. Fig. 1(e) shows the elemental distribution, indicating that nitrogen and oxygen are uniformly doped in the carbon shell, with a small amount of iron possibly being residual iron oxide or carbon-iron compounds. The internal hollow space and porosity of CS850-4.5 contribute to its high BET surface area and pore volume.

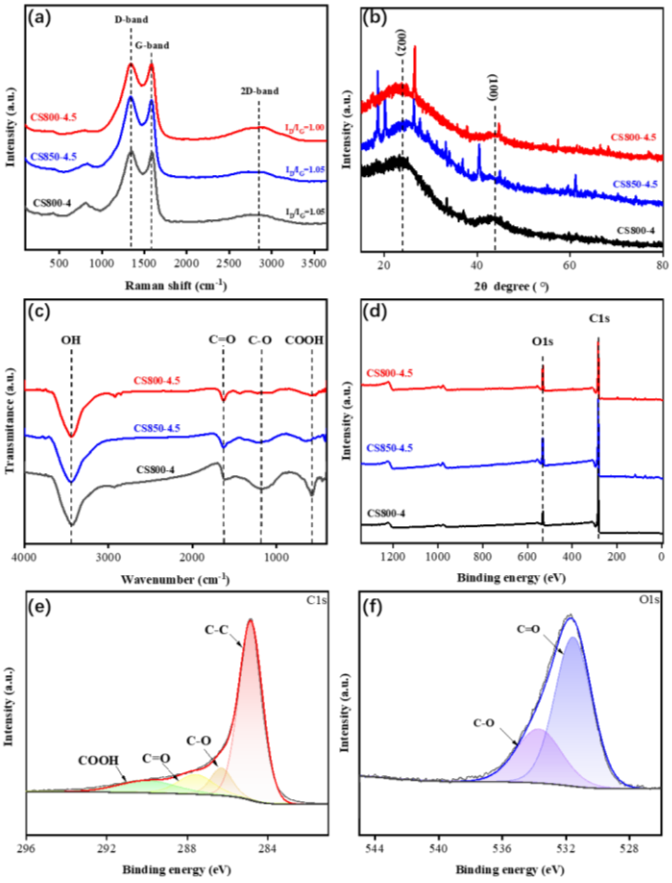

Fig. 2. (a) Raman spectra; (b) XRD pattern; (c) FTIR spectrum; (d) XPS survey spectrum; (e, f) High-resolution XPS spectra of C1S and O1S for CS850-4.5.

In Fig. 2(a), the Raman spectra of CS800-4.5,CS850-4.5, and CS800-4 show prominent peaks at 1346 cm^{-1} (D band) and 1588 cm^{-1} (G band), along with a 2D peak. The I_D/I_G values of 1.0, 1.05, and 1.05 indicate that the materials are predominantly amorphous carbon. This is further supported by the XRD patterns in Fig. 2(b), which display broad diffraction peaks at 2θ = 24° and 44°, corresponding to the (002) and (100) planes of graphite. The broad peaks suggest the presence of disordered structures within the non-graphitic carbon, such as the random distribution of carbon layers.

The FTIR spectra in Fig. 2(c) reveal the C–OH stretch band and C–O vibration at approximately 3440 cm^{-1} and 1100 cm^{-1} for the three samples. Additionally, there is a clear C=O peak near 1630 cm^{-1}, and a COOH peak at 640 cm^{-1}. Further XPS analysis, as shown in Fig. 2(d), indicates that the primary elements in the materials are carbon and oxygen. The surface oxygen contents (wt%) are 17.54% (CS800-4.5), 14.60% (CS800-4), and 20.47% (CS850-4.5), all of which are higher than the oxygen content typically found in conventional activated carbon (2-11%).

In Fig. 2(e), the C 1s peaks appear to consist of four components. The C–C single bond is observed at 284.83 eV, while the C–O single bond and C=O double bond are located at 286.19 eV and 287.38 eV, respectively, corresponding to the peaks at 531.01 eV and 532.28 eV in the O 1s spectra shown in Fig. 2(f). The presence of COOH groups is consistent with the observations in Fig. 2(a).Abundant oxygen-containing functional groups in CS850-4.5 are anticipated to enhance the number of adsorption sites available for hydrogen molecules.[7]

3.3. Pore Structure and Pore Size Analysis

Hydrogen storage in porous carbon requires materials with the highest surface area and appropriately sized pores.

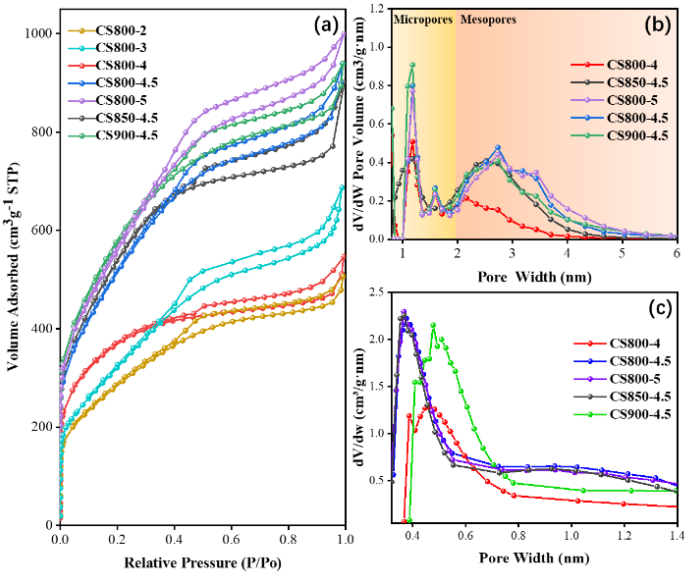

Fig. 3. (a) N2 adsorption-desorption isotherms; (b) Pore size distribution from the DFT method; (c) Micropore size distribution from the HK method.

The nitrogen adsorption isotherms, shown in Fig. 3(a), initially display a Type I isotherm characteristic of microporous materials, followed by a transition to a Type II isotherm. This behavior indicates that N_2 molecules rapidly fill the micropores and then form multilayer adsorption in the mesopores and hollow regions of the spheres as pressure increases. Additionally, adsorption hysteresis is observed, with the hysteresis loop resembling an H4 type, suggesting that the pores formed in the material are primarily narrow slit-shaped micro-mesopores.

The pore size distribution of the five samples was analyzed using the DFT and HK methods. As shown in Fig. 3(b). The samples exhibit a similar pore size distribution, with micropores predominantly peaking at 1.2 nm and mesopores ranging from 2.5 nm to 2.7 nm. Notably, CS800-4 and CS900-4.5 show a higher concentration of micropores at 0.8 nm. Except for CS850-4.5, the other samples also present a minor peak at 1.6 nm. As shown in Fig. 3(c), the primary sizes of ultramicropores are 0.37 nm (CS800-4.5, CS800-5, CS850-4.5) and 0.48 nm (CS800-4, CS900-4.5). The micropore size distribution of CS850-4.5 corresponds closely with the results observed in the TEM analysis.

3.4. Hydrogen Storage Analysis

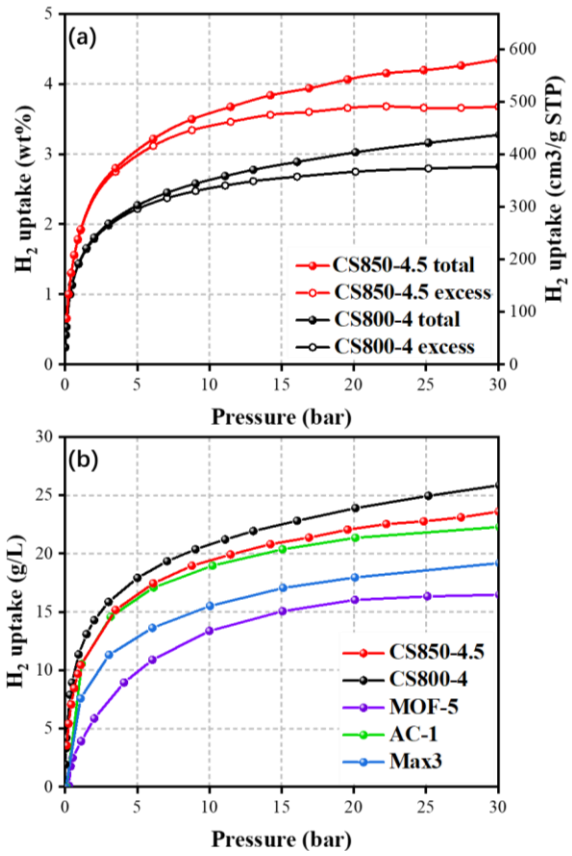

Fig. 4. (a) Gravimetric hydrogen adsorption isotherms for CS800-4 and CS850-4.5; (b) Volumetric hydrogen adsorption isotherms for CS800-4 and CS850-4.5, compared with commercially available highly porous adsorbents MOF-5, Max3 (Maxsorb 3000), and AC-1 (KOH-activated anthracite).[8]

Table 2 H2 uptake of CS800-4 and CS850-4.5

Sample	Pore size (nm)	ρ_s (cm3/g)	H_2 uptake(wt%)		H_2 uptake (g/L)
			1bar	30bar	30bar
CS800-4	0.8/1.2	2.4	1.5	3.3	25.9
CS850-4.5	1.2/2.5	2.2	1.9	4.3	23.6

As shown in Fig. 4(a), the hydrogen adsorption isotherms for CS800-4 and CS850-4.5 exhibit a Langmuirian shape, indicating the significant role of micropores in the adsorption process. The hydrogen adsorption is reversible and without hysteresis, suggesting efficient adsorption and desorption. At 30 bar, the total hydrogen adsorption amounts for CS800-4 and CS850-4.5 reached 3.3 wt% and 4.3 wt%, respectively. For CS850-4.5, tests at 50 bar demonstrated that hydrogen adsorption met the U.S. Department of Energy's 2020 requirement for onboard hydrogen storage materials (4.5 wt%). However, as the pressure increased beyond 25 bar, the excess adsorption for CS800-4 and CS850-4.5 began to decline, indicating that the gas density in the pores does not increase proportionally with the overall hydrogen density. This results in negative excess adsorption. Thus, the optimal operating pressure for these materials is 25 bar.

According to Table 2, CS800-4 has pore sizes concentrated between 0.5 nm and 0.8 nm, which are considered most favorable for hydrogen adsorption at 77K and ambient pressure.[9] However, due to its relatively low BET surface area and total volume, the hydrogen adsorption capacity only reaches 1.5 wt% at 1 bar. In contrast, CS850-4.5 has a micropore surface area of 1522 m^2/g and a micropore volume of 1.00 m^3/g. The presence of numerous 1–2 nm micropores correlates with enhanced hydrogen uptake capacity under high-pressure conditions[10], resulting in a modest hydrogen uptake of 2.3 wt% at 1 bar and high hydrogen uptake 4.5 wt% at 50 bar. Additionally, the micropore-mesopore structure of the hollow carbon spheres facilitates rapid

transfer of hydrogen molecules to the micropores of the inner surfaces, enhancing adsorption encapsulation.

Considering that volumetric adsorption capacity (g/L) is a critical evaluation metric for practical applications, especially within confined volumes, the volumetric adsorption capacities of CS800-4 and CS850-4.5 were calculated using the general formula for packing density:[7]

$$\rho_p = (\rho_s{}^{-1} + V_{total})^{-1}$$

$$H_2\ uptake\ (g/L) = H_2\ uptake\ (wt\%) \times \rho_p$$

The packing densities of CS800-4 and CS850-4.5 were determined to be 0.79 g/cm³ and 0.54 g/cm³, respectively. As shown in Fig. 4(b), CS800-4, despite its lower H_2 uptake, achieves a higher volumetric H_2 uptake (25.9 g/L) than CS850-4.5 (23.6 g/L) and commercial adsorption materials such as Max3, AC-1, and MOF-5. Additionally, CS800-4's lower activation temperature and ratio suggest reduced production costs. Both CS800-4 and CS850-4.5 demonstrate significant potential as hydrogen storage materials.

4. CONCLUSIONS

In this study, we prepared a series of hollow porous carbon spheres using biogas slurry as a raw material, varying factors such as activation temperature and KOH-to-CS mass ratio during the activation phase. CS850-4.5, with an activation temperature of 850°C and an activation ratio of 4.5, features a high BET surface area (2140 m²/g), micropore area (1522 m²/g), and micropore volume (1 cm³/g), along with an oxygen content of 20.47%. It achieved a hydrogen adsorption capacity of 4.5 wt% at 77 K and 50 bar. Additionally, CS800-4 and CS850-4.5 demonstrated high volumetric adsorption capacities (25.9 g/L and 23.6 g/L, respectively) due to their relatively high packing densities. These findings provide new insights into the development of cost-effective hydrogen storage materials and the efficient processing of biogas slurry.

ACKNOWLEDGEMENT

This work is supported by the National Key R&D Program of China (2018YFC1903204).

DECLARATION OF INTEREST STATEMENT

The authors declare that they have no known competing financial interests or personal relationships that could have appeared to influence the work reported in this paper. All authors read and approved the final manuscript.

REFERENCE

[1] Gao, Y. et al. Experimentally validated design principles of heteroatom-doped-graphene-supported calcium single-atom materials for non-dissociative chemisorption solid-state hydrogen storage. Nat Commun 15 (2024) 928.

[2] Boateng, E. & Chen, A. Recent advances in nanomaterial-based solid-state hydrogen storage. Materials Today Advances 6 (2020) 100022.

[3] Ball, M. & Wietschel, M. The future of hydrogen – opportunities and challenges. International Journal of Hydrogen Energy 34 (2009) 615–627.

[4] Ke, L. et al. Component analysis and risk assessment of biogas slurry from biogas plants. Chinese Journal of Chemical Engineering 44 (2022) 182–191.

[5] Cai, T. et al. Superhigh-rate capacitive performance of heteroatoms-doped double shell hollow carbon spheres. Carbon 86 (2015) 235–244.

[6] Zarezadeh Mehrizi, M., Abdi, J., Rezakazemi, M. & Salehi, E. A review on recent advances in hollow spheres for hydrogen storage. International Journal of Hydrogen Energy 45 (2020) 17583–17604.

[7] Blankenship, L. S., Balahmar, N. & Mokaya, R. Oxygen-rich microporous carbons with exceptional hydrogen storage capacity. Nat Commun 8 (2017) 1545.

[8] A comparison of hydrogen storage in activated carbons and a metal–organic framework (MOF-5). Carbon 48 (2010) 2906–2909.

[9] Bosu, S. & Rajamohan, N. Recent advancements in hydrogen storage - Comparative review on methods, operating conditions and challenges. International Journal of Hydrogen Energy 52 (2024) 352–370.

[10] Yang, S. J. et al. General Relationship between Hydrogen Adsorption Capacities at 77 and 298 K and Pore Characteristics of the Porous Adsorbents. J. Phys. Chem. C 116 (2012) 10529–10540.